



HAL
open science

A centerline based model morphing algorithm for patient-specific finite element modelling of left ventricle

Sareh Behdadfar, Laurent Navarro, Joakim Sundnes, Molly M Maleckar, S. Ross, H.H. Odland, Stéphane Avril

► To cite this version:

Sareh Behdadfar, Laurent Navarro, Joakim Sundnes, Molly M Maleckar, S. Ross, et al.. A centerline based model morphing algorithm for patient-specific finite element modelling of left ventricle. *IEEE Transactions on Biomedical Engineering*, 2017. hal-01671488

HAL Id: hal-01671488

<https://hal.science/hal-01671488v1>

Submitted on 22 Dec 2017

HAL is a multi-disciplinary open access archive for the deposit and dissemination of scientific research documents, whether they are published or not. The documents may come from teaching and research institutions in France or abroad, or from public or private research centers.

L'archive ouverte pluridisciplinaire **HAL**, est destinée au dépôt et à la diffusion de documents scientifiques de niveau recherche, publiés ou non, émanant des établissements d'enseignement et de recherche français ou étrangers, des laboratoires publics ou privés.

A Centerline Based Model Morphing Algorithm for Patient-Specific Finite Element Modelling of the Left Ventricle

S. BEHDADFAR*, L. NAVARRO, J. SUNDNES, M. MALECKAR, S. ROSS, H. H. ODLAND and S. AVRIL

Abstract— Goal: Hexahedral automatic model generation is a recurrent problem in computer vision and computational biomechanics. It may even become a challenging problem when one wants to develop a patient-specific finite-element (FE) model of the left ventricle (LV), particularly when only low resolution images are available. In the present study, a fast and efficient algorithm is presented and tested to address such a situation. **Methods:** A template FE hexahedral model was created for a LV geometry using a General Electric (GE) ultrasound (US) system. A system of *centerline* was considered for this LV mesh. Then, the nodes located over the endocardial and epicardial surfaces are respectively projected from this centerline onto the actual endocardial and epicardial surfaces reconstructed from a patient’s US data. Finally, the position of the internal nodes is derived by finding the deformations with minimal elastic energy. This approach was applied to eight patients suffering from congestive heart disease. A FE analysis was performed to derive the stress induced in the LV tissue by diastolic blood pressure on each of them. **Results:** Our model morphing algorithm was applied successfully and the obtained meshes showed only marginal mismatches when compared to the corresponding US geometries. The diastolic FE analyses were successfully performed in seven patients to derive the distribution of principal stresses. **Conclusion:** The original model morphing algorithm is fast and robust with low computational cost. **Significance:** This low cost model morphing algorithm may be highly beneficial for future patient-specific reduced-order modelling of the LV with potential application to other crucial organs.

Index Terms—Model morphing, Numerical simulation, EchoPac® ultrasound imaging, Cardiac modelling.

I. INTRODUCTION

In spite of recent advances in medical imaging and image processing, constructing a patient-specific finite-element

(FE) mesh of the left ventricle (LV) remains daunting. In addition to the challenges of accurately reconstructing patient anatomy, numerical simulations of cardiac mechanics put strict demands on mesh quality and regularity, as illustrated in [1]. Another issue is that automatic geometry extraction usually provides surface data (STL format). Often, the volume surrounded by this surface can be simply meshed with tetrahedral elements. One example of such method is integrated in General Electric (GE) Healthcare ultrasound (US) system named EchoPac® software. The LV is reconstructed in triangulated elements which can be easily converted into tetrahedral meshes [2].

However, a critical problem arises in meshing an organ with hexahedral elements, the standard choice in 3D solids thanks to their numerical and computational efficiency and accuracy, especially if a large number of patients have to be processed within a reasonable timeframe [3]. Their shape functions, directional sizing without loss, accurate connectivity and decrease in overall elements population in comparison to tetrahedral meshes are the proven essential properties of such elements [3]-[4]. In addition, it is easy to consider a local coordinate system for such elements to determine the anisotropic material behavior of the LV in FE codes. However, in order to generate automatically hexahedral elements, one requires a precise knowledge of element shape functions and nodal connectivity in mesh domain which might not be available.

In addition to these meshing methods, NURBS-based elements may also be employed with great potential [5]. An example of such methods was previously developed to reconstruct personalized meshes using cubic elements with a Hermite shape function [1]. The proposed method wraps a predefined NURBS-based high quality template mesh onto the registered images. This interpolation requires a wrapping field from nodal positions and the derivatives of the shape function to the local coordinates [6]. However, the success of mesh wrapping intrinsically depends both on the level of image resolution as well as the number of control points appropriately employed. Bad image quality, wrong choice of control points, presence of noise and inaccurate wrapping field may be possible causes of wrapping failure or overfitting. We suggest a new approach which overcomes these difficulties for low resolution images by directly projecting a template mesh,

*S. Behdadfar is with Mines Saint-Etienne, CIS-EMSE, SAINBIOSE, F-42023; INSERM, U1059, and Université de Lyon, SAINBIOSE, F-42000 Saint Etienne, France (e-mail: behdadfar.sareh@gmail.com).

L. Navarro and S.Avril are with Mines Saint-Etienne, CIS-EMSE, SAINBIOSE, F-42023; INSERM, U1059, and Université de Lyon, SAINBIOSE, F-42000 Saint Etienne, France.

J. Sundnes is with Simula Research Laboratory and Center for Cardiological Innovation, Dept. of Cardiology, Oslo University Hospital, Oslo, Norway.

M. Maleckar is with ALLEN institute for cell science. S. Ross and H.H Odland are with Center for Cardiological Innovation, Dept. of Cardiology, Oslo University Hospital, Oslo, Norway.

called the reference deformable FE (RDFE) model, onto a subject's geometry.

The paper is organized as following: the new approach is introduced in Section II. In Section III, this proposed method is used to morph a deformable LV model meshed in hexahedral elements onto the geometry of eight subjects for whom US images were acquired in triangulated surfaces. In Section IV, the FE models reconstructed for these subjects are employed to derive the distribution of principal stresses in the LV wall. Finally, the potential benefits and also some limitations of the presented method are discussed in Section V before concluding in Section VI.

II. METHODS

A. Introduction to the methodology

Model morphing and deformable shape registration [7]-[9] are commonplace in medical computational modelling [10]-[11]-[13]-[14]-[15] and computer vision [12]-[24]-[25]-[26]-[27].

Here, we developed an algorithm that can address situations in which the template model and the target geometry have a different structure. We considered an available healthy geometry of a human LV for this purpose instead of a truncated ellipsoid or other generic data, as this method is insensitive to the geometry of the reference data. The three stages of the algorithm are described in the following sections:

- 1: Reference Rigid Transformation: align basal surfaces.
- 2: Nonrigid Transformation: register only the nodes located on the boundaries of the template RDFE model.
- 3: Intermediate Node Deformation.

B. Rigid Body Registration Method

Two geometries are available for this application: a template geometry, the RDFE model, meshed with hexahedral elements (bulk volume) and a target subject specific geometry, meshed only with triangular elements at its boundaries

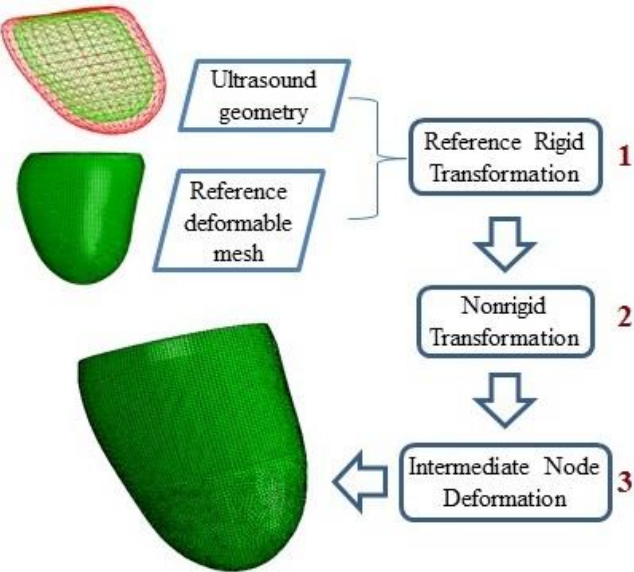


Fig. 1. Proposed model morphing pipeline which is outlining the three steps of rigid and nonrigid transformation.

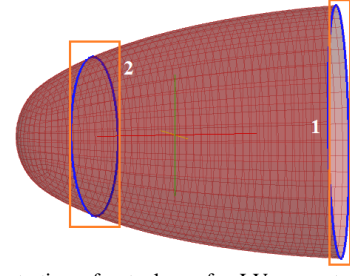


Fig. 2. An illustration of cut planes for LV geometry. The equatorial plane 1 forms the basal surface and plane 2 defines the spherical part (apex).

(meshed surface).

Let (\mathbf{P}_i^{Ne}) ($i \in [1,3]$) denote the position vectors of a set of nodes defining a triangle on the basal surface (refer to Fig.2) of the template RDFE geometry. Then we define the template unit normal vector as:

$$\mathbf{N}^{Ne} = (\mathbf{P}_2^{Ne} - \mathbf{P}_1^{Ne}) \times (\mathbf{P}_3^{Ne} - \mathbf{P}_1^{Ne}). \quad (1)$$

The target surface is made of Ne' elements with Np' nodes. Let $\mathbf{P}'_i^{Ne'}$ be the position vectors of a set of nodes defining a triangle perpendicular to the main axis of the LV (this main axis is obtained by a singular value decomposition of the nodal coordinates). The plane defined by these three nodes is the basal plane of the target geometry. Then we define the target unit normal vector such as:

$$\mathbf{N}'^{Ne'} = (\mathbf{P}'_2^{Ne'} - \mathbf{P}'_1^{Ne'}) \times (\mathbf{P}'_3^{Ne'} - \mathbf{P}'_1^{Ne'}). \quad (2)$$

Given that: $Ne' \ll Ne$ and $Np' \ll Np$.

Using Rodrigues' formula [28], we define successfully (Eqs 3 to 6): the normalized rotation vector of basal normals (axis of rotation) \mathbf{RV} , the cross product matrix $\overline{\mathbf{RV}}$, the anticlockwise angle θ about the axis $\overline{\mathbf{RV}}$ and the rotation matrix R .

$$\mathbf{RV} = -(\mathbf{N}'^{Ne'} \times \mathbf{N}^{Ne}) / \|\mathbf{N}'^{Ne'} \times \mathbf{N}^{Ne}\|, \quad (3)$$

$$\overline{\mathbf{RV}} = \begin{bmatrix} 0 & -\mathbf{RV}(3) & \mathbf{RV}(2) \\ \mathbf{RV}(3) & 0 & -\mathbf{RV}(1) \\ -\mathbf{RV}(2) & \mathbf{RV}(1) & 0 \end{bmatrix}, \quad (4)$$

$$\cos\theta = (\mathbf{N}'^{Ne'} \cdot \mathbf{N}^{Ne}) / (\|\mathbf{N}'^{Ne'}\| \|\mathbf{N}^{Ne}\|), \quad (5)$$

$$R = I + \sin\theta \overline{\mathbf{RV}} + (1 - \cos\theta) \overline{\mathbf{RV}}^2. \quad (6)$$

Then we rotate the RDFE mesh with the R matrix to align it with the target mesh.

C. Nonrigid Registration Method for the Boundaries

We define two points to define the centerline of the RDFE model: the first point is at the barycenter of the RDFE basal surface and the second one is at the barycenter of the apical surface (refer to Fig.2). The centerline is only defined for the

RDFE mesh since it will be used to project nodes of the RDFE model onto the target surface.

From this *centerline*, for every node of the RDFE mesh, we consider another vector, denoted **Ray**, normal to the centerline and passing through each RDFE node. This **Ray** points towards the target surface. For each RDFE node, we derive the intersection of **Ray** and the target surface using the triangle intersection algorithm proposed by [29]. This algorithm takes the vertices $T(V_1, V_2, V_3)$ of each triangle from the target surface and examines whether the current **Ray** from the RDFE centerline to the RDFE current node intersects it or not on its trajectory.

We know that the intersection point of **Ray** and the triangle, denoted by **Int**, should lie in the plane of the triangle. Therefore, we can write a system of equations (7) and (8).

$$T(a, b) = (1 - a - b)V_1 + aV_2 + bV_3, \quad (7)$$

$$\mathbf{Int} = O + t\mathbf{D}. \quad (8)$$

where $T(a, b)$ is the barycenter coordinates of the current triangle; t is the distance (unknown) from the **Ray** origin O to the intersection point **Int** with direction \mathbf{D} .

Then we need to solve the equation $T(a, b) = \mathbf{Int}$:

$$O + t\mathbf{D} = (1 - a - b)V_1 + aV_2 + bV_3, \quad (9)$$

Denoting $\mathbf{e}_1 = V_2 - V_1$ and $\mathbf{e}_2 = V_3 - V_1$, equation (9) can be rewritten as:

$$[\mathbf{D} \ \mathbf{e}_1 \ \mathbf{e}_2] \begin{bmatrix} t \\ a \\ b \end{bmatrix} = O - V_1, \quad (10)$$

Based on Cramer's rule:

$$\begin{bmatrix} t \\ a \\ b \end{bmatrix} = 1/|-\mathbf{D} \ \mathbf{e}_1 \ \mathbf{e}_2| \begin{vmatrix} \mathbf{S} & \mathbf{e}_1 & \mathbf{e}_2 \\ -\mathbf{D} & \mathbf{S} & \mathbf{e}_2 \\ -\mathbf{D} & \mathbf{e}_1 & \mathbf{S} \end{vmatrix}. \quad (11)$$

where $\mathbf{S} = O - V_1$.

Solving (11) gives three parameters (t, a, b) which should fulfill several conditions. The first condition is that **Ray** should intersect the triangle. We begin by calculating the determinant $det = \mathbf{e}_1 \cdot (\mathbf{Ray} \times \mathbf{e}_2)$ and if the determinant is below 1×10^{-5} , the **Ray** is parallel to the triangle.

Then, we calculate $u = det^{-1}(\mathbf{Ray} \times \mathbf{e}_2) \cdot (\mathbf{Ray}_{origin} - V_1)$ and $v = det^{-1}\mathbf{Ray} \cdot ((\mathbf{Ray}_{origin} - V_1) \times \mathbf{e}_1)$. If $(u, v) < 0$ and $(u, u+v) > 1$, the intersection lies outside of the triangle. Finally, two triangles are found candidates which one is on the correct direction of the current **Ray**. The correct intersection position should be on the line from centerline to the RDFE node ($t > 0$). This process is repeated for all the RDFE surface nodes and the 3D coordinates of intersection points are saved (Fig.3). The epicardial RDFE surface nodes were also projected on the respective target surface.

The presented approach outlined in Section II.B-C was developed using an in-house program coded in MATLAB®.

D. Registration Method Across the Bulk Volume

In the previous section, we defined the method to project surface nodes of the RDFE model onto the target geometry. However, it does not provide the deformation to be applied to the nodes located inside the RDFE model and not on its boundary surfaces. In order to deform the intermediate nodes across the bulk, the displacements of the RDFE boundaries are used to define a classical linear elastic Dirichlet problem on the continuous RDFE 3D volume. We refer to Hooke's law of basic continuum mechanics [30]-[31]:

$$\sigma = C \ \varepsilon. \quad (12)$$

where C is the fourth-order elasticity tensor, ε is the elastic deformation and σ is the Cauchy stress tensor.

Boundary conditions for the Dirichlet problem are the known displacements of the RDFE surface determined as explained in the previous section:

$$U = \bar{u}. \quad (13)$$

where \bar{u} is the prescribed displacement vector on the boundaries $\partial\Omega_u$. Vector \bar{u} connects each RDFE node to its projection on the target geometry.

III. APPLICATION ON COHORT DATA

To validate our approach we applied it to the LV of 8 patients and performed FE stress analyses with the obtained morphed meshes.

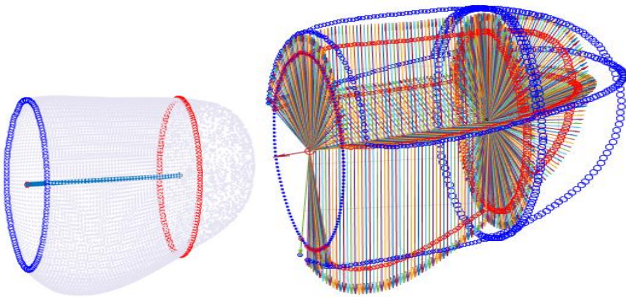


Fig. 3. The figure shows: left, the centerline which connects the center of apex edge of LV to the center of basal part. The basal and apical planes are shown in blue and red circles on the LV body. Right, several projections of reference nodes in red to the target surface in blue from defined centerline.

A. Data Acquisition

To reconstruct the RDFE geometry, the LV of a healthy volunteer was segmented at end-diastole (ED) from EchoPac® (GE Healthcare) [2]. Then, the RDFE model was precisely created with 8-noded linear brick (hexahedral) elements with $Np = 155,172$ nodes and $Ne = 141,405$ elements by Abaqus® software tools. The cavity and tissue volumes of this model were 89.3 and 112.6 ml, respectively.

Imaging data from eight heart failure patients with left bundle branch block (LBBB) eligible for cardiac resynchronization therapy (CRT) were obtained from the Impact study [32]. LV geometries (Fig.4) were measured throughout the cardiac cycle with cardiac US, and post processing of the US images were performed in the Echopac® Software (GE Healthcare) at admission to the Hospital. Pressure curves were acquired during the implantation procedure of the CRT with an indwelling left ventricular transcutaneous intracardiac pressure catheter (MicroCath, Millar Instruments). Pressure curves were stored in the LabChart data acquisition software (Adinstruments Inc.).

The target geometries were closed surfaces of endocardium and epicardium which were meshed with triangulation algorithm in EchoPac® [2]; $Np' = 1282$ nodes and $Ne' = 2558$ elements, precisely the situation described in Section II.B: $Ne' \ll Ne$ and $Np' \ll Np$.

B. Model Morphing Method Application on Cohort

We registered and projected the RDFE boundaries to each

patient as explained above (Section II.B-C). The continuum deformation of intermediate nodes is modelled with elastic properties of Young's modulus and Poisson's ratio equal to 2×10^6 MPa and 0.35, respectively. These material parameters provided a reasonable deformation of RDFE 3D model to the target geometries. To arrive at this parameterization, we ran several simulations with different Young's moduli and Poisson's ratios to study the deformation of RDFE model and compared the morphed results with patient's surfaces. This process was performed using FE Abaqus® software (a multimedia file has been provided to show this step for Case #1). As the RDFE geometry is an open cavity surface, the final expected result is a morphed open cavity with the bulk LV tissue of patient data.

C. Cohort Diastolic Phase FE Simulation

We applied the developed model morphing method on all patients' geometries at early diastole and ED (see Fig.5 for early diastole) in their pressure-volume curve at contraction and relaxation phases, respectively.

For the diastolic phase, we used the Guccione strain energy function W for a nearly incompressible and transversely isotropic material model [33], developed in Abaqus® software with parameters in Table I [34]. The strain energy function W may be written as:

$$W = c(\exp(Q) - 1)/2 + U(J), \quad (14)$$

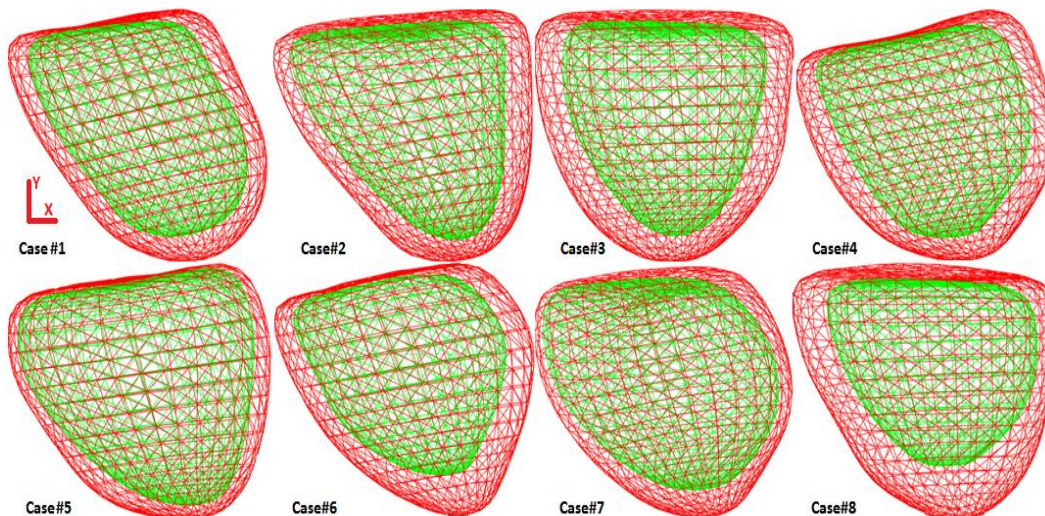


Fig. 4. The LBBB patient geometries obtained from EchoPac® postprocessing on GE US data. The endocardial and epicardial surfaces shown in green and red, respectively, for early diastole instance.

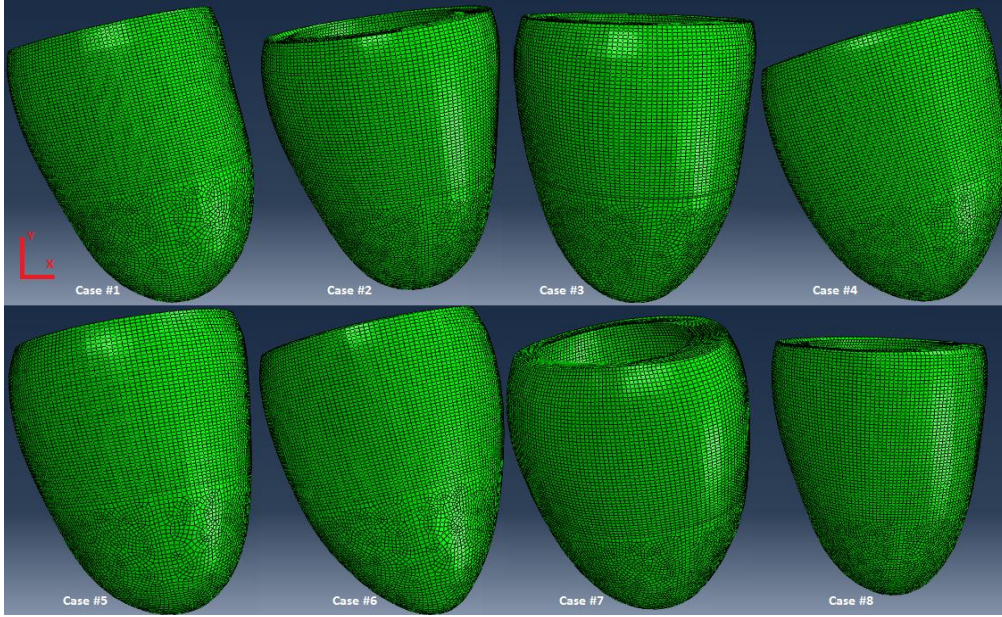


Fig. 5. The figure shows the application of developed model morphing method on LBBB patient geometries obtained from EchoPac® US at early diastole instance.

where Q is:

$$Q = b_1 \bar{E}_{ff}^2 + b_2 (\bar{E}_{ss}^2 + \bar{E}_{nn}^2 + 2\bar{E}_{sn}^2) + b_3 (2\bar{E}_{fs}^2 + 2\bar{E}_{fn}^2). \quad (15)$$

where, c and $b_{1,3}$ are the material parameters, \bar{E}_{ij} are the components of the distortional Green-Lagrange strain tensor in the local coordinate system in *fiber*, *sheet* and *normal to sheet* directions, and $U(J)$ is the volumetric part of the strain energy function [35]. $U(J)$ in the FE simulation was defined as a function of bulk modulus K and with J which is the determinant of the deformation gradient.

$$U(J) = K((J^2 - 1)/2 - \ln(J))/2. \quad (16)$$

A local curvilinear coordinate system aligned along the fiber direction was considered to model myocyte directions based on [36]. It was assumed that myofibres run parallel to the surfaces (imbrication angle equal to zero). Fiber directions varied from 60° at the endocardial surface to -70° at the epicardial surface, where 0° is the circumferential direction.

In order to avoid rigid body motion in FE simulations, the basal nodes were allowed to deform radially. We applied the corresponding patient's cavity pressure (refer to Table II) from early diastole to the ED to the endocardial surface and performed diastolic simulations. The diastole phase is where the ventricular tissue is relaxed and the oxygenated blood

TABLE I
MATERIAL PARAMETERS

c (Pa)	b_1	b_2	b_3	K (kPa)
512	67.1	24.2	21.6	0.1

TABLE II
INTRACAVITAL PRESSURE OBTAINED FROM LBBB PATIENTS

Case	#1	#2	#3	#4	#5	#6	#7	#8
Pressure (kPa)	3.2	4	1.333	3.2	0.4	3.6	1.84	3.466

enters to the LV cavity.

IV. RESULTS

The method outlined in Fig.1 was applied for all patients in Fig.4, as shown in Fig.5.

The registration and projection methods for each surface (MATLAB®) took less than 10 min on a 2 core PC (Intel i5-4590 3.3 GHz 8Go RAM) and the intermediate deformation (Abaqus®) takes about 5 min on 8 cores (Intel Xeon X5650 2.67 GHz 24Go RAM). The total process for each patient uses approximately 25 min of wall time.

An illustration of the diastolic phase is shown in Fig.6. For Cases #1, #2, #4, #6, and #8, we observed a homogenous distribution of principal stresses through the wall thickness which highlights the high quality of the morphed elements. In Cases #3 and #5, we noticed several elements at both base and apex which have different values than their surroundings. This shows that the methodology can be quite sensitive to the conical shape of the apex in terms of the quality of deformed elements. The basal differences in these cases might be due to the applied boundary conditions to the basal nodes which limit some degrees of freedom for rigid body deformation for diastolic simulations. Case #7 had no convergence success due to the LV extremely thin wall thickness and subsequently distorted elements.

Table III contains the intracavitary volume obtained from FE ED simulations and patient's data. There are small differences in final intracavitary volume which is due to the tissue material parameters.

In Table IV, we report the following metrics about mesh quality: the aspect ratio, the minimum angle on the hexahedral faces, the maximum angle on the hexahedral faces and the elements' minimum edge length. For each of the 8 patients, the extreme values (worst value across the whole ventricular volume with 141,405 elements) and the average value of each metrics are reported. Extreme values reported in Table IV reasonably remain in a range of sufficient mesh quality for a

TABLE III
EARLY DIASTOLE AND ED CAVITY VOLUME

Volume (ml) \ Case	#1	#2	#3	#4	#5	#6	#8
ED (EchoPac®)	163	168	168	154	319	151	112
ED (FE)	166	164	167	128	266	174	98
early diastole	113	144	133	106	233	103	78

TABLE IV
MESH AND ELEMENT QUALITY TEST

Metric values \ Case	#1	#2	#3	#4	#5	#6	#7	#8
Worst aspect ratio	4.69	4.30	6.78	25	32	9.95	82	9.45
Mean aspect ratio	1.61	1.61	1.55	1.65	2.35	1.78	2.27	1.82
Worst min angle on quad faces (°)	7.6	3.41	5.16	11.3	1.45	25.5	0.58	16
Mean min angle on quad faces (°)	73.2	71.5	69	71	64.9	71	64	74
Worst max angle on quad faces (°)	181	181	193	181	202	167	231	186
Mean max angle on quad faces (°)	107	109	111	109	115	109	117	107
Mean min edge length (mm)	0.71	0.71	0.78	0.72	0.78	0.87	0.84	0.76

finite-element analysis. Only 2 cases had elements with an aspect ratio above 10. However, for one of them (Case #5), the worst minimum and maximum angles were similar to the other cases and the element with the worst aspect ratio did not bring trouble for the linear elastic finite-element analysis of Case #5 (ill-conditioning of the stiffness matrix due distorted elements was not reported). Finally, Case #7 was the only case with poor mesh quality, showing a worst aspect ratio of 82 and extreme minimum and maximum angles significantly smaller and larger, respectively, than the values of the other cases.

V. DISCUSSION

In general, nonrigid registration is a challenging problem and it is dependent on the input data. It is also treated as a nonlinear optimization problem [37], [38], [27]. However, the local optimization methods may become stuck in local optima if not properly initialized. A better option can be a global optimization algorithm that does a complete search to find the global solution.

Here, we developed a novel approach for simple patient-specific nonrigid transformation of biological organs without considering it as an optimization problem. We avoid these optimization difficulties and overfitting problems as discussed in [1]. The advantage is that our algorithm did not need physical correspondence on both geometries for projection and additionally produced meaningful, physiologically relevant results. It also does not require *a priori* assumption or constraints to project the RDFE 3D surface to the target surface. The ability to ignore target mesh problems as gaps, overlaps and holes is one of the important properties of this developed approach. However, the optimization methods become more interesting when the reference geometry is too coarse and its mesh does not precisely represent the target geometry.

We have developed a method to morph a deformable LV

model to patient LV data in the case where RDFE and target meshes are very different in density. Previously, [39] developed a centerline method for arteries. It worked by moving a Voronoi sphere on the average centerline of the artery and finding the intersect positions of this sphere with the target shape. Their developed approach is valid on topologies close to the arteries and is not applicable to conical shapes such as the LV. Our developed method is also based on the centerline of the LV, but instead we project the RDFE nodes from this centerline to the target surface.

Several methods have been developed for volumetric deformation, such as different models of heat kernel signature or heat diffusion processes on a shape [40]-[43], wave heat kernel signature based on quantum mechanics [44] and differential deformation schemes [45]. These methods require a sufficient knowledge of these fields for their correct application.

The linear elastic transformation method has been used previously for this purpose in the literature [46]-[49]. Authors of [50] reviewed and compared the application of elastic transformation in medical imaging and continuum mechanics problems. In order to deform the RDFE solid model with intermediate nodes, we used elastic body deformation using FE simulation. It is applicable using any FE software and simple to develop without precise knowledge of continuum mechanics and FE simulation in detail which is an advantage for computer vision or clinical use.

Material properties were chosen to obtain a reasonable intermediate node deformation. The Young's modulus and Poisson's ratio have an important impact on the model behavior of the FE geometry. If the material is compliant, the boundaries deform and the internal nodes remain at their initial positions. The FE elastic simulation had the best results with high Young's modulus and relatively medium Poisson's ratio values.

The FE simulations on the morphed RDFE models were successful except for Case #7 which had no convergence success due to the LV wall thickness and low mesh quality. Indeed, the relatively small wall thickness of this model (refer to the Fig.4-Case#7 and Table IV), particularly on the left hand side of this geometry, made this FE simulation be unsuccessful. We also noted in Table IV that Case #7 had the poorest mesh quality, probably due to the very thin wall which caused distortion of RDFE model elements in the attempt to fit to the target boundaries. One solution to this problem might be to iteratively adapt the local thickness of the RDFE mesh by a scaling factor in order to prevent such extreme distortions.

The application of this method is fast, efficient, and simple to implement as a pipeline. It takes less than 25 minutes to morph a RDFE model to the target surfaces with the help of MATLAB® and Abaqus® software.

A. Limitations and Future work

One disadvantage of this method is that during the elastic deformation, some elements remained without volume due to the variation in wall thickness and the nature of RDFE

element type (hexahedral). This situation was observed in Case #7. In the intermediate node deformation, we perform a FE simulation once, and the model deforms. In this case, the elements can reach their limits of deformation or can become smaller due to the Poisson's ratio value. It is not critical itself, but becomes critical if another FE simulation is started from this resulting mesh, in which the morphed geometry can fail to achieve FE convergence such as in Case #7. It was necessary, in this case, to remove these elements which were concentrated on the endocardial apex and basal boundaries manually as a post-processing step for diastolic FE simulations. This choice is justified due to the importance of elements at domain boundaries for intracavitary applied pressure which are highly sensitive to the element's quality. This issue has been observed in [1] as well. It is also the cause for generated stress heterogeneities at the apex and basal regions in Cases #3, #5 and #6. We have noticed that the zones related to the removed elements fits to these heterogeneities.

Another limitation is that this method is based on a centerline projection; so, if the geometry has several layers, they should be treated separately with their RDFE corresponding surfaces. In this paper, we treated the endocardial and epicardial surfaces separately from their reference centerlines to the target surfaces.

In the data available for our study, fiber directions were not experimentally measured. Our work was devoted to ultrasound data for which the material structure cannot easily be derived. Here, as proposed by [33], we assigned fiber angles varying from -70° to 60° across the ventricular wall. But future work, potentially involving diffusion MRI, will consider the generation of patient-specific material structure [51]-[52].

As future work, one might apply this method on biventricular or complete heart meshes to verify its feasibility and reproducibility on shape analysis and computer vision problems. In case of biventricular geometries, a potential improvement is to define two centerlines each for the LV and right ventricle for both endocardium and epicardium, and then to project the reference surfaces. This will be much more

challenging if the complete heart is considered, due to the importance of the centerline definition. Then, one could define a complex network of centerlines in a complete heart. Here, we examined the developed methodology specifically on LV morphology alone.

Another improvement may be to identify the strain energy function material parameters for each patient with their pressure volume curves to achieve more meaningful results during the diastolic FE application. Lack of constraint in this manner likely explains differences in the final ED volume from patient's data and the FE simulations in Table III. The importance of material parameters for exponential strain energy function has been discussed in [53]. In Case #5, the discrepancy in the ED volumes is due to the construction of the basal plane in our method, which does not lie at the same location as the endocardial surface closing provided by the Echopac system.

One interesting improvement to this study would be to validate the viability of the present method during the systolic phase of LV for the available patient cohort as proposed in [1].

Another improvement would also be to couple ultrasound imaging with other imaging modalities in order to better capture the complete myocardial tissue [54].

VI. CONCLUSION

In this paper, a new methodology was presented to morph a deformable generic model onto a patient-specific geometry in the case where the density of the generic mesh is at least 10 times larger than the density of the available nodes for the patient-specific geometry. The method showed very promising results for patient-specific FE analyses of the LV on a cohort of patients suffering from LBBB disease. It is now ready to be used in a patient-specific simulation pipeline based on medical imaging techniques. It could also be applied to different organ systems such as arteries, brain, and bones.

ACKNOWLEDGEMENTS

The authors gratefully acknowledge the support and data provided by the Center for Cardiological Innovation, funded

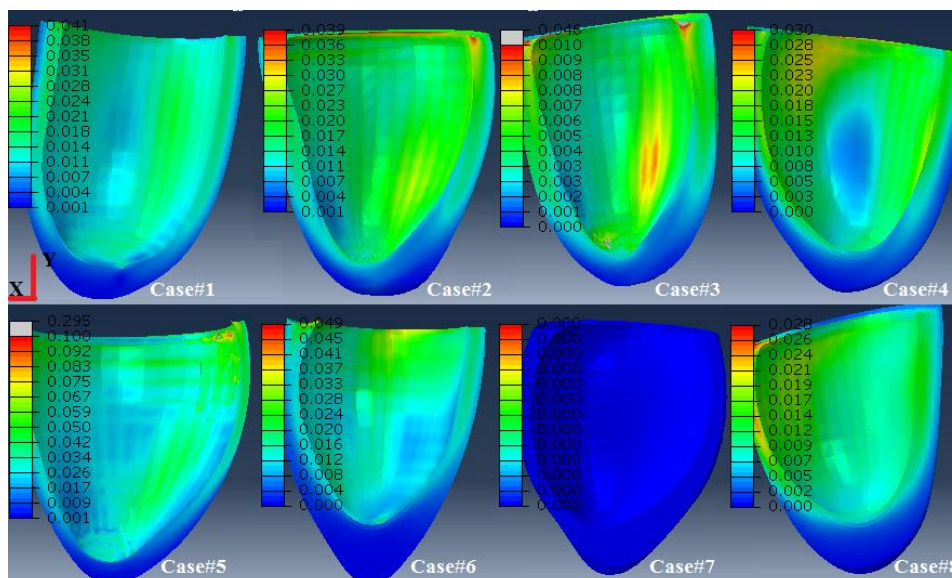


Fig. 6. The maximum principal stresses results of ED FE simulations. Case #7 did not converge in these FE simulations.

by the Research Council of Norway. S. Avril is grateful to the European Research Council for grant ERC-2014-CoG BIOLOCHANICS.

REFERENCES

- [1] P. Lamata *et al.*, “An accurate, fast and robust method to generate patient-specific cubic Hermite meshes,” *Medical image analysis*, vol. 15, no 6, p. 801-813, 2011.
- [2] J. Hansegård *et al.*, “Semi-automated quantification of left ventricular volumes and ejection fraction by real-time three-dimensional echocardiography,” *Cardiovascular ultrasound*, vol. 7, no 1, p. 1, 2009.
- [3] T. Blacker, “Meeting the challenge for automated conformal hexahedral meshing”, *9th international meshing roundtable, pages 11–20. Citeseer, 2000.*
- [4] S. E. Benzley, E. Perry, K. Merkley, B. Clark, and G. Sjaardama, A comparison of all hexagonal and all tetrahedral finite element meshes for elastic and elasto-plastic analysis. In *Proceedings, 4th International Meshing Roundtable, volume 17, pages 179–191. Sandia National Laboratories Albuquerque, NM. 1995.*
- [5] T. Marin and J. G. Brankov, “Deformable left-ventricle mesh model for motion-compensated filtering in cardiac gated SPECT”. *Medical physics*, vol. 37, no 10, p. 5471-5481, 2010.
- [6] P. Lamata, S. Niederer, D. Barber, D. Norsletten, J. Lee, R. Hose, and N. Smit. “Personalization of cubic hermite meshes for efficient biomechanical simulations”. In *International Conference on Medical Image Computing and Computer-Assisted Intervention, pages 380–387. Springer 2010.*
- [7] N. J., Mitra *et al.*, “Dynamic geometry registration,” *Symposium on geometry processing*, p. 173-182, 2007.
- [8] Q. X. Huang *et al.*, “Non-Rigid Registration Under Isometric Deformations,” *Computer Graphics Forum*, Blackwell Publishing Ltd, p. 1449-1457, 2008.
- [9] H. Li *et al.*, “Global Correspondence Optimization for Non-Rigid Registration of Depth Scans,” *Computer graphics forum*, Blackwell Publishing Ltd, p. 1421-1430, 2008.
- [10] M. A. Audette *et al.*, “An algorithmic overview of surface registration techniques for medical imaging,” *Medical image analysis*, vol. 4, no 3, p. 201-217, 2000.
- [11] Y. Liu, “A mean field annealing approach to accurate free form shape matching,” *Pattern Recognition*, vol. 40, no 9, p. 2418-2436, 2007.
- [12] G. K. Tam *et al.*, “Registration of 3D point clouds and meshes: a survey from rigid to nonrigid. Visualization and Computer Graphics,” *IEEE Transactions on*, vol. 19, no 7, p. 1199-1217, 2013.
- [13] P. Piras, A. Evangelista, S. Gabriele, P. Nardinocchi, L. Teresi, C. Torromeo *et al.*, “4D-analysis of left ventricular heart cycle using Procrustes motion analysis,” *PloS one*, 9(1), e86896, 2014.
- [14] P. Piras, C. Torromeo, F. Re, A. Evangelista, S. Gabriele, G. Esposito *et al.*, “Left Atrial trajectory impairment in Hypertrophic Cardiomyopathy disclosed by Geometric Morphometrics and Parallel Transport,” *Scientific Reports*, 6, 2016.
- [15] A. Madeo, P. Piras, F. Re, S. Gabriele, P. Nardinocchi, L. Teresi, A. Evangelista *et al.*, “A new 4D trajectory-based approach unveils abnormal LV revolution dynamics in hypertrophic cardiomyopathy,” *PloS one*, 10(4), e0122376, 2015.
- [16] S. Rusinkiewicz and M. Levoy, “Efficient variants of the ICP algorithm,” 3-D Digital Imaging and Modelling, Proceedings. Third International Conference on. IEEE, p. 145-152, 2001.
- [17] B. Amberg *et al.*, “Optimal step nonrigid icp algorithms for surface registration,” *Computer Vision and Pattern Recognition, CVPR'07. IEEE Conference on. IEEE*, p. 1-8, 2007.
- [18] C. Papazov *et al.*, “Deformable 3D shape registration based on local similarity transforms,” *Computer Graphics Forum*, vol. 30, no. 5, p. 1493-1502, Aug. 2011.
- [19] D. C. Barber *et al.*, “Efficient computational fluid dynamics mesh generation by image registration,” *Medical image analysis*, vol. 11, no 6, p. 648-662, 2007.
- [20] B. Couteau *et al.*, “The mesh-matching algorithm: an automatic 3D mesh generator for finite element structures,” *J. of biomechanics*, vol. 33, no 8, p. 1005-1009, 2000.
- [21] A. P. Gibson *et al.*, “A method for generating patient-specific finite element meshes for head modelling,” *Physics in medicine and biology*, vol. 48, no 4, p. 481, 2003.
- [22] J. W. Fernandez *et al.*, “Anatomically based geometric modelling of the musculo-skeletal system and other organs,” *Biomechanics and modelling in mechanobiology*, vol. 2, no 3, p. 139-155, 2004.
- [23] M. Bucki *et al.*, “A fast and robust patient specific finite element mesh registration technique: application to 60 clinical cases”. *Medical image analysis*, vol. 14, no 3, p. 303-317, 2010.
- [24] X. Li and I. Guskov, “Multiscale Features for Approximate Alignment of Point-based Surfaces,” *Symposium on geometry processing*, p. 217-226, 2005.
- [25] I. A. Sigal *et al.*, “Mesh-morphing algorithms for specimen-specific finite element modelling,” *J. of biomechanics*, vol. 41, no 7, p. 1381-1389, 2008.
- [26] O. Van Kaick *et al.*, “A survey on shape correspondence,” *Computer Graphics Forum*. Blackwell Publishing Ltd, p. 1681-1707, 2011.
- [27] A. Myronenko and X. Song, “Point set registration: Coherent point drift. Pattern Analysis and Machine Intelligence,” *IEEE Transactions on*, vol. 32, no 12, p. 2262-2275, 2010.
- [28] O. Rodriguez, “Des lois geometriques qui regissent les déplacements d'un systeme solide dans l'espace et de la variation des coordonnees provenant de déplacements consideres independamment des causes qui peuvent les produire,” *J Math Pure Appl*, vol. 5, p. 380-440 , 1840.
- [29] T. Möller *et al.*, “Fast, minimum storage Ray/triangle intersection,” *ACM SIGGRAPH Courses*, p. 7, July, 2005.
- [30] G. A. Holzapfel, “Nonlinear solid mechanics: A continuum approach for engineering science,” *Meccanica*, 2002, vol. 37, no 4, p. 489-490.
- [31] J. Bonet, and R. D. Wood, “Nonlinear continuum mechanics for finite element analysis”. *Cambridge university press, 1997.*
- [32] Oslo University Hospital, Acute feedback on left ventricular lead implantation location for cardiac resynchronization therapy (CCI impact), <https://clinicaltrials.gov>, 2016.
- [33] J. M. Guccione *et al.*, “Passive material properties of intact ventricular myocardium determined from a cylindrical model,” *J. of biomechanical engineering*, vol. 113, no 1, p. 42-55, 1991.
- [34] R. J. Okamoto *et al.*, “Epicardial suction: a new approach to mechanical testing of the passive ventricular wall.” *J. of biomechanical engineering* 122.5: 479-487, 2000.
- [35] G. A. Ateshian and K. D. Costa, “A frame-invariant formulation of Fung elasticity,” *J. of biomechanics*, vol. 42, no 6, p. 781-785, 2009.
- [36] J. M. Huyghe *et al.*, “Porous medium finite element model of the beating left ventricle,” *American Journal of Physiology-Heart and Circulatory Physiology*, 262(4), H1256-H1267, 1992.
- [37] A. Lorusso *et al.*, *A comparison of four algorithms for estimating 3-D rigid transformations*, University of Edinburgh, Department of Artificial Intelligence, 1995, pp. 237-246.
- [38] Y. Sahillioglu and Y. Yemez, “Minimum-distortion isometric shape correspondence using EM algorithm,” *Pattern Analysis and Machine Intelligence, IEEE Transactions on* 34.11: 2203-2215, 2012.
- [39] L. Antiga, “Patient-specific modelling of geometry and blood flow in large arteries”. *Politecnico di Milano, 2002.*
- [40] J. Sun *et al.*, “A Concise and Provably Informative Multi-Scale Signature Based on Heat Diffusion,” *Computer graphics forum*, Blackwell Publishing Ltd, vol. 28, no. 5, p. 1383-1392, 2009.
- [41] M. Ovsjanikov *et al.*, “One point isometric matching with the heat kernel,” *Computer Graphics Forum*. Blackwell Publishing Ltd, p. 1555-1564, 2010.
- [42] M. M. Bronstein and I. Kokkinos, “Scale-invariant heat kernel signatures for non-rigid shape recognition,” *Computer Vision and Pattern Recognition (CVPR), IEEE*, 2010.
- [43] D. Raviv *et al.*, “Affine-invariant diffusion geometry for the analysis of deformable 3D shapes,” *arXiv preprint arXiv:1012.5933*, 2010.
- [44] M. Aubry *et al.*, “The wave kernel signature: A quantum mechanical approach to shape analysis,” *Computer Vision Workshops (ICCV Workshops), IEEE*, 2011.
- [45] H. Zhang *et al.*, “Deformation-Driven Shape Correspondence,” *Computer Graphics Forum*. Blackwell Publishing Ltd, p. 1431-1439, 2008.
- [46] C. Broit, “Optimal registration of deformed images,” Ph.D. dissertation, Dept. Comput. Inf. Sci., Univ. Pennsylvania, Philadelphia, 1981.
- [47] R. Bajcsy *et al.*, “A computerized system for the elastic matching of deformed radiographic images to idealized atlas images,” *J. of computer assisted tomography*, vol. 7, no 4, p. 618-625, 1983.
- [48] C. Davatzikos and R. N. Bryan, “Using a deformable surface model to obtain a shape representation of the cortex,” *Medical Imaging, IEEE Transactions on*, 15(6), 785-795, 1996.

- [49] C. Davatzikos, "Spatial transformation and registration of brain images using elastically deformable models," *Computer Vision and Image Understanding*, vol. 66, no 2, p. 207-222.
- [50] M. Holden, "A review of geometric transformations for nonrigid body registration," *Medical Imaging, IEEE Transactions on*, vol. 27, no 1, p. 111-128, 2008.
- [51] L. Zhukov *et al.*, "Heart-muscle fiber reconstruction from diffusion tensor MRI," *In Visualization, 2003. VIS 2003. IEEE (pp. 597-602). IEEE 2003.*
- [52] P. Basser *et al.*, "In vivo fiber tractography using DT-MRI data," *Magnetic resonance in medicine*, 44(4), 625-632, 2000.
- [53] S. Behdadfar, *et al.*, "Importance of material parameters and strain energy function on the wall stresses in the left ventricle," *Computer Methods in Biomechanics and Biomedical Engineering*, 1-10, 2017.
- [54] J. Pedrosa *et al.*, "Left Ventricular Myocardial Segmentation in 3-D Ultrasound Recordings: Effect of Different Endocardial and Epicardial Coupling Strategies," *IEEE transactions on ultrasonics, ferroelectrics, and frequency control*, 64(3), 525-536, 2017.